Photodiagnosis and Photodynamic Therapy 34 (2021) 102329

Contents lists available at ScienceDirect

Photodiagnosis and Photodynamic Therapy

journal homepage: www.elsevier.com/locate/pdpdt

Surface-enhanced Raman spectroscopy analysis of serum samples of typhoid patients of different stages

Maimoona Tahira [a], Haq Nawaz [a,*], Muhammad Irfan Majeed [a,*], Nosheen Rashid [b], Shaheera Tabbasum [a], Muhammad Abubakar [a], Shamsheer Ahmad [a], Saba Akbar [a], Saba Bashir [a], Muhammad Kashif [a], Saqib Ali [a], Hamza Hyat [a]

[a] Department of Chemistry, University of Agriculture Faisalabad, Faisalabad, 38040, Pakistan
[b] Department of Chemistry, University of Central Punjab, Faisalabad Campus, Faisalabad, Pakistan

ARTICLE INFO

Keywords:
Typhoid fever
Salmonella typhi
SERS
Serum
Multivariate data analysis
Raman spectroscopy

ABSTRACT

Background: Surface-enhanced Raman spectroscopy (SERS) of body fluids is considered a quick, simple and easy to use method for the diagnosis of disease.
Objectives: To evaluate rapid, reliable, and non-destructive SERS-based diagnostic tool with multivariate data analysis including principal component analysis (PCA) and partial least square discriminant analysis (PLS-DA) for classification of different stages of typhoid on the basis of characteristic SERS spectral features.
Methods: SERS has been used for analysis of serum samples of different stages of typhoid including early acute stage and late acute stage in comparison with healthy samples, in order to investigate capability of this technique for diagnosis of typhoid. SERS spectral features associated with the biochemical changes taking place during the development of the typhoid fever were analyzed and identified.
Results: The value of area under the receiver operating characteristics (AUROC) for early acute stage versus healthy is 0.87 and that for healthy versus late acute stage is 0.52. PLS-DA classifier model gives values of 100 % for accuracy, sensitivity and specificity, respectively for the SERS spectral data sets of healthy versus early acute stage. Moreover, this classifier model gives values of 91 %, 89 % and 97 % for accuracy, sensitivity and specificity, respectively for the SERS spectral data sets of healthy versus late acute stage.
Conclusions: Based on preliminary work it is concluded that SERS has potential to diagnose various stages of typhoid fever including early acute and late acute stage in comparison with healthy samples.

1. Introduction

Typhoid fever is an infectious [1], contagious [2], and life-threatening disease [3]. The pathogen of this disease is sub-specie *Salmonella enterica serovar typhi* [4], which is a gram-negative, host-adapted, human-specific pathogen and belongs to the rod-shaped, aerobic, and flagellated bacterial family named *Enterobacteriaceae* [5]. Typhoid fever is considered a significant factor for the cause of morbidity and mortality [6,7] in the global distribution due to the emergence of 21.6 million cases annually. This disease is a monsoonal fever and its rate of perfusion is high during rainy days and can cause its outbreak.

Enteric fever is characterized by abdominal pain, persistent fever & headache, vomiting, paradoxical bradycardia, atrophy, drowsiness, loss of appetite, redness, and intestinal pain. Other symptoms are neurological include inflammation of the spinal cord and catalepsy [8]. Due to inducing systematic infection in humans, *Salmonella* subspecies are recognized as a leading contributor to bloodstream infections. These clinical symptoms fall into ranges from less complicated high-grade fever to more complicated and serious illness leading towards hemorrhage, peritonitis, encephalopathy, and perforation. Typhoid is rare in developed countries but remains a serious health problem in areas of poor sanitary and unhygienic conditions [9]. *S. typhi* is water-borne obligate and mode of transmission are person-to-person, contaminated water and food [10], visit endemic areas, shellfish, fruit, and vegetables harvested from soil subjected to human waste and sewage-contaminated water defecation in open places [11].

Although different microbial and serological techniques such as

* Corresponding authors.
E-mail addresses: haqchemist@yahoo.com (H. Nawaz), irfan.majeed@uaf.edu.pk (M.I. Majeed).

https://doi.org/10.1016/j.pdpdt.2021.102329
Received 17 February 2021; Received in revised form 14 April 2021; Accepted 30 April 2021
Available online 6 May 2021
1572-1000/© 2021 Elsevier B.V. All rights reserved.

blood culture [12], Enzyme-linked immune-sorbent assays (ELISA) [13,14], biosensors [15], Loop-mediated isothermal amplification [16,17], immunofluorescence [18], Polymerase Chain Reaction (PCR) [19], Widal test for characteristic antigens [20,21], duodenal string culture [22], lateral flow immunoassay [23] are used to diagnose typhoid fever, they are subjected to limitations of low specificity and time-consuming [24]. Moreover, it is difficult to discriminate enteric fever from other diseases such as paratyphoid (A, B, C) and pneumonia because of similarity in prolonged fever and other clinical manifestations which demand sensitive, precise, reproducible, and accurate methods for the diagnosis. Raman spectroscopy is identified as a potential candidate for the identification of water-borne. It is inexpensive, providing wider information content, having high analytical speed on chemical composition, structure, and bio-molecular interactions within microorganisms. Raman spectroscopy is a type of vibrational molecular spectroscopy and can help in quantitative and qualitative analysis of samples [25]. Apart from being rapid, simple, and sensitive, Raman spectroscopy is subjected to weak signal intensity. It also faces some problems in the identification of biological fluids containing low concentration such as serum, plasma, synovial fluid in joints and lymph. Surface-Enhanced Raman spectroscopy has the potential to detect a low concentration of biological fluids due to the enhancement of Raman signal caused by the nanoparticles as substrates [26]. Clinically, there is a need to analyze early acute stage and late acute stage typhoid so that a proper treatment can be provided to early acute stage patients therefore our technique can be used for the diagnosis of different stages of typhoid fever and their comparison for the characterization of the biochemical changes associated with the development of the severity of this disease due to its high sensitivity and specificity. The utility of this technique as a clinical tool can also be extended for the diagnosis of other diseases at different stages.

Previously, Raman Spectroscopy has been reported to differentiate healthy and typhoid serum. They have acquired Raman spectra with laser power of 150 mW and the changes they found to differentiate healthy and typhoid samples are at 630 cm^{-1}, 1099 cm^{-1}, 1144 cm^{-1}, 1343 cm^{-1}, 1692 cm^{-1}, 1711 cm^{-1}, and 1746 cm^{-1} that are very minor changes and hard to identify visually [27]. The Raman fingerprints of unknown sample will not be characteristic/unique enough to identify either that sample belongs to healthy or infected individual that is why, it cannot be employed to differentiate different stages of typhoid that require more sensitivity of a technique. In the current study, Surface-enhanced Raman Spectroscopy (SERS) is employed with laser power of only 90 mW to analyze serum samples of two stages of typhoid including early acute stage and late acute stage as compared to the healthy samples. We have obtained greater number of characteristic features that differentiate healthy and typhoid samples as compared to normal Raman (NR). Also, we have successfully employed SERS for the differentiation of different stages of typhoid. It is observed that the concentration of IgM (immunoglobulin M) increases at the early acute stage. *S. typhi* is intracellular at this stage and not directly present in serum, but biochemical changes associated with typhoid fever can be observed by taking serum as a target analyte for diagnosis. With time, *S. typhi* flows in bloodstream and becomes extracellular. At that point, the late acute stage appears and the concentration of IgG (immunoglobulin G) increases along with IgM. A critical review of the previous literature has shown that no such comparison is published yet.

2. Materials and methods

2.1. Serum isolation from the blood of typhoid patients

On removal of cells and blood clotting agents from blood, the remaining liquid part of blood is known as serum and should therefore contain proteins and other molecules which represent the entire body system [28]. The whole blood sample was obtained in a blood collecting tube and centrifugal separation was performed to separate blood components to obtain serum. All samples were collected from Allied Hospital Faisalabad, Pakistan. A total of 60 samples were obtained including 20 healthy, 20 of the early acute stage, and 20 of the late acute stage of typhoid serum samples.

2.2. Synthesis of silver nanoparticles and substrate for SER measurements

Ag NPs were synthesized by chemical reduction method using silver nitrate ($AgNO_3$) as a precursor and tri-sodium citrate ($Na_3C_6H_5O_7$) as reducing agent and capping ligand as we previously described [29]. More briefly, 0.0085 g/300 mL of silver nitrate solution in distilled water is heated at 100 °C then 10 mL of 1 % tri-sodium citrate is introduced. The solution is boiled for one and half hours on a hot plate along with magnetic stirring to obtain the grey-colored silver nanospheres [30].

2.3. Characterization of Ag-NPs

Characterization of obtained Ag NPs was carried out by transmission and scanning electron microscopy (TEM and SEM) using a field emission electron microscope (JEOL, JSM-7500F) as described in our previous publication [29]. Briefly, for TEM, the samples were prepared by slow evaporation of a drop from an aqueous suspension of Ag NPs onto a carbon-coated copper grid (400 mesh). For SEM, dried Ag NPs were placed on a copper stub without any extra conductive coating. ImageJ software was used to analyze the electron micrographs.

2.4. SERS measurements

For this purpose, 30 μL of each sample was mixed with 30 μL of silver nanoparticles and left for 30 min as incubation time to develop good interaction between sample and nanoparticles. The longer incubation time let nanoparticles interact sufficiently with the sample and the distance between nanoparticles and sample decreases. The electromagnetic strength increases with the close binding of nanoparticles and it results in the strong SERS intensity of healthy and typhoid samples. The SERS spectra have been recorded after every 10 min and we observed that the incubation time of 30 min provides good results that is why this incubation time was fixed for all measurements [31,32]. From this incubation mixture, 40 μL of typhoid positive and healthy individuals was placed on an aluminum slide and SERS spectral acquisition was performed using Raman spectrometer (ATR8300BS, Optosky, China). For this purpose, a 785 nm diode laser was used as an excitation source by delivering laser power of 90 mW through a 40 X objective, and an air-cooled charged coupled device (CCD) detector was used to record Raman scattering. For all the serum samples, 15 Raman spectra were acquired in the spectral range of 200 to 1800 cm^{-1} with an acquisition time of 10 s.

2.5. SERS spectral data pre-processing

All Raman spectral data of typhoid infected and healthy human serum was pre-processed by using MATLAB 7.8 and established protocols. By taking all the SERS spectral data in a matrix, different preprocessing steps involving smoothing, substrate removal, correction of baseline, and vector normalization were carried out. Savitzky-Golay (13 peekpoint window, 3rd order polynomial) standardization technique has been utilized to smooth raw spectral information content. For the elimination of the baseline, a rubber band correction was evaluated out for every spectrum. The best indication of baseline correction is that the spectrum starts from zero and finally ends at zero.

2.6. Data analysis

In the current study, multivariate data analyses such as Principal Component Analysis (PCA) and Partial Least Square Discriminate

Table 1
SERS peak assignments of spectral data of healthy and typhoid positive serum samples.

SERS Shift (cm^{-1})	Peak assignments	Healthy Serum	Typhoid Early acute stage	Typhoid Late acute stage	References
440	N-C-S stretch (thiocyanate)	✓	x	x	[36]
456	Ring torsion of phenyl	x	x	✓	[37]
496	Glycogen, C-N-C deformation	✓	✓	✓	[38,39]
533	Cholesterol ester		✓	✓	[40]
595	Phosphatidylinositol	✓	✓	✓	[40]
562/649	Uric acid	✓	✓	X	[41]
730	Lipids	✓	✓	X	[42]
814	C-C stretching (collagen assignment)	✓	✓	x	[43]
890	Protein bands	✓	✓	✓	[44,45]
961	Phosphate symmetric stretching vibration of calcium hydroxyapatite	✓	✓	✓	[46]
1005	Phenylalanine (proteins)	✓	✓	✓	[47]
1047	Glycogen	✓	X	x	[48]
1099	Palmitic acid	x	✓	x	[43]
1105	Carbohydrates peak for solutions	x	✓	✓	[49]
1140	Alpha amylase	✓	✓	✓	[50]
1206	Hydroxyproline, tyrosine	✓	✓	✓	[42]
1330	Region associated with DNA & phospholipids Collagen	x	✓	✓	[51]
1362	Tryptophan	✓	X	x	[52]
1455	Deoxyribose	x	X	✓	[53]
1590	Carbon particles	x	X	✓	[54]
1623	Tryptophan (IgG)	x	✓	✓	[43]
1652	Lipid (C═C stretch)	x	X	✓	[38]
1691	Amide I (turns and bands)	x	X	✓	[55]
1701	C═O (lipid)	✓	X	✓	[56]

Analysis (PLS-DA) were employed for the analysis of SERS spectral data of healthy serum and two stages of typhoid (early acute stage and late acute stage) serum samples. PCA is an unsupervised method and a mathematical procedure involving the transformation of possibly correlated variables into a smaller number of uncorrelated variables, known as principal components (PCs), to reduce the dimensionality of the data whilst maintaining their variability. The dominant source of variability in data is accounted by the first principal component (PC-1) and each succeeding principal component is counted for the further highest source of remaining variability. The PC loading could be understood as orthogonal dimensions of variability which facilitate the differentiation of different groups of Raman spectral data along with their coefficient as each spectrum of serum sample of typhoid fever and healthy scores along these dimensions [33]. The Partial Least Square Discriminant Analysis (PLS-DA) is a classifier model and combination of Partial Least Square & Partial Discriminate Analysis and both these approaches are supervised. PLS-DA model is a statistical tool that has the potential to predict, classify, and explain as well to differentiate the variability among the groups. Furthermore, it has the advantage to explain the multi-dimensional dataset for various purposes such as diagnosing different stages of disease in the medical field, analyzing product quality assurance, and investigating forensic medical examination [34]. The area under the receiver operating characteristics is mostly used to check the diagnostic accuracy of the classifier model and measure the usefulness of the technique. It is a graphical representation plotted against the true positive rate and the false positive rate. The true positive rate represents sensitivity and the false positive rate shows specificity. Furthermore, it is the likelihood that a randomly chosen individual with the disorder will score higher on the test than a randomly chosen individual without the disorder [35].

3. Results

Electron microscopy revealed Ag NPs to be of oval geometry with an average size of 65 × 45 nm as shown in Fig. (S1). The SERS results were interpreted by using Raman spectral features assignments taken from

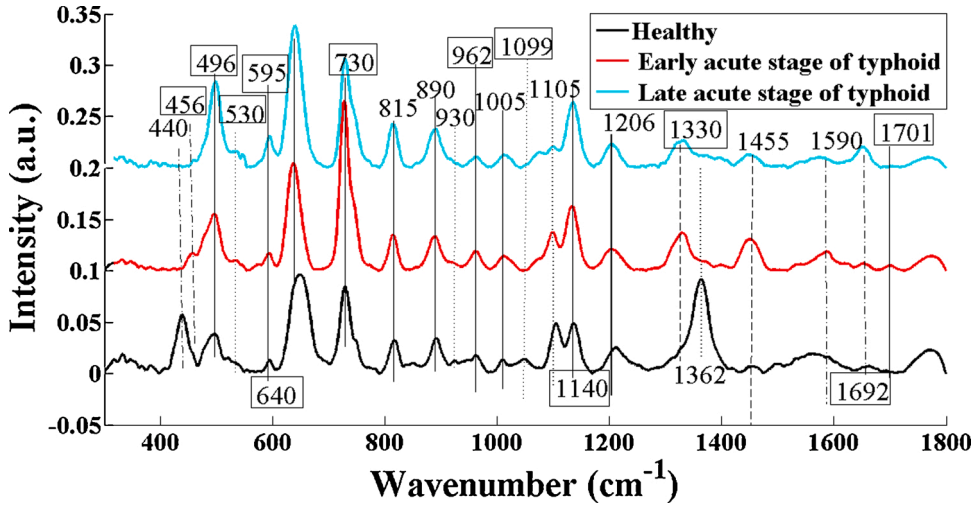


Fig. 1. Mean SERS spectra of healthy serum (Black) versus two stages of typhoid (early acute stage (red) and late acute stage (cyan)).

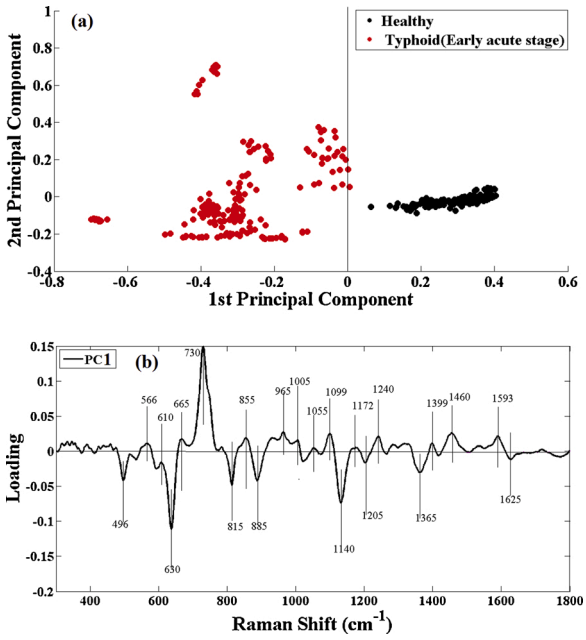


Fig. 2. (a) PCA Scatter plot of SERS spectral data of Healthy (black) and early acute stage (red) (b) Loadings of PCA of SERS spectral data of Healthy versus early acute stage of typhoid serum.

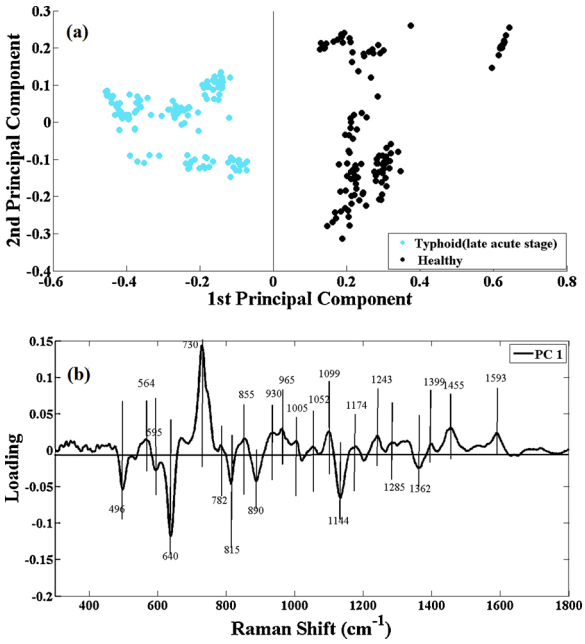


Fig. 3. (a) PCA Scatter plot of SERS spectral data of Healthy (black) compared with the late acute stage (cyan) (b) Loadings of PCA of Healthy versus Late acute stage of typhoid serum samples.

literature, and are assigned in Table 1. Fig. 1 shows the mean SERS spectra of serum samples of healthy versus two stages of typhoid (early acute stage and late acute stage). The SERS peaks appearing in healthy serum show different patterns as compared to typhoid (early acute stage and late acute stage) positive serum.

Here, comparison of healthy and two stages of typhoid serum were done through mean SERS spectra. The features including 440 cm^{-1}, 496 cm^{-1}, 533 cm^{-1}, 640 cm^{-1}, 730 cm^{-1}, 815 cm^{-1}, 960 cm^{-1}, 1005 cm^{-1}, 1099 cm^{-1}, 1005 cm^{-1}, 1140 cm^{-1}, 1330 cm^{-1}, 1362 cm^{-1} and 1455 cm^{-1} are observed as prominent changes and discussed here one by one.

The Peaks labeled with boxes can be considered as characteristic features associated with the development of typhoid. The Peak observed at 456 cm^{-1} is due to δ (C-C) Ring torsion of phenyl. Raman peak at 496 cm^{-1}, 530 cm^{-1}, and 595 cm^{-1} could be associated with cholesterol ester, Phosphatidylinositol, and C-N-C deformation, respectively. Two bands of phosphate backbone (C—C) (lipids) at 1099 cm^{-1} and 1701 cm^{-1} may be contributions from the symmetric deoxyribose stretching and C═O stretching of lipid molecules, respectively. SERS bands observed at 562 and 649/640 cm^{-1} are reported for the presence of uric acid. Lipid characteristic peak at wavenumber 730 cm^{-1} is observed [57], 1099 cm^{-1} (palmitic acid) [58], 1399 cm^{-1} and 1556 cm^{-1} represents high density lipoproteins (HDL) [59]. Raman band at 1140 cm^{-1} is a representation of alpha-amylase [50]. At 1330 cm^{-1}, a band is observed in the mean SERS spectrum of typhoid serum samples and represents CH_3 and CH_2 wagging (proteins/lipids) [60]. Raman band at 1692 cm^{-1} may be contributions of DNA (Z-form) [55] and dT C2═O stretching vibrations [61]. Along with these, it can be proposed that Raman shift at 1701 cm^{-1} arises due to cholesterol esters or triglycerides [62]. Moreover, peaks at 440 cm^{-1} N-C-S stretch (thiocyanate) and 1362 cm^{-1} (tryptophan) were observed only in healthy serum samples. On the other hand, a peak at 1099 cm^{-1} (Palmitic acid) was identified only in early acute typhoid.

3.1. Principal Component Analysis (PCA)

Principal Component Analysis (PCA) is performed so that each unknown sample could be differentiated based on the associated biochemical changes. PCA has been applied on SERS spectral data sets of diseased samples including early acute stage and late acute stage of typhoid and healthy serum samples.

Fig. 2 (a) shows PCA scatter plot showing the variability of SERS spectral data of diseased and healthy samples. Each cluster at a different location is the indication that variability among different kinds of samples is observed. Here each dot represents one spectrum.

The spectral data associated with the healthy serum samples is clustered on the negative side of the PC-1 (black color) of healthy are grouped indicate that they are similar at a molecular level and varied from each other clusters which have different kinds of spectral features from other Early acute typhoid grouped on the right side/positive side of the PC-1 shown as a red cluster. The scatter plot of various samples is helpful to explain variability in different groups and also among the samples of the same group.

Fig. 2 (b) shows loadings of PCA of SERS spectral data of early acute stage of typhoid and healthy samples. The negative loadings of PC-1 can be associated with spectral data of early acute stage of typhoid serum samples include 496 cm^{-1}, 533 cm^{-1}, 595 cm^{-1}, 640 cm^{-1},815 cm^{-1}, 890 cm^{-1}, 1005 cm^{-1}, 1099 cm^{-1}, 1140 cm^{-1}, 1285 cm^{-1}, 1366 cm^{-1}, 1418 cm^{-1} and 1630 cm^{-1} and loadings in positive side including 730 cm^{-1}, 854 cm^{-1}, 958 cm^{-1}, 1020 cm^{-1}, 1202 cm^{-1}, 1392 cm^{-1}, 1455 cm^{-1} and 1587 cm^{-1} can be associated with spectral data of healthy serum samples grouped in the positive axis of the PC-1. Major variations are explained by PC-1 as 87 %, and the remaining 13 % explained by PC-2. These observations of negative and positive loadings are similar to the mean SERS spectra of the infected blood serum and healthy ones, respectively.

Fig. 3 (a) shows PCA scatter plot of Raman spectral data sets of the late acute stage of typhoid (cyan dots) and healthy serum samples (black dots) and shows that both sets of SERS spectral data are clustered in the negative and positive axis of PC-1, respectively. There are strong variations at different Raman shifts of these data sets reflected in the form of their clustering separately.

In the Fig. 3 (b), the positive loadings including 730 cm^{-1}, 855 cm^{-1}, 930 cm^{-1}, 965 cm^{-1}, 1005 cm^{-1}, 1052 cm^{-1}, 1099 cm^{-1}, 1174 cm^{-1}, 1243 cm^{-1}, 1399 cm^{-1}, 1455 cm^{-1}, and 1593 cm^{-1} can be related with the Raman spectra of healthy serum samples, grouped in the positive axis of the PC-1 and loadings in negative side including 496 cm^{-1}, 564

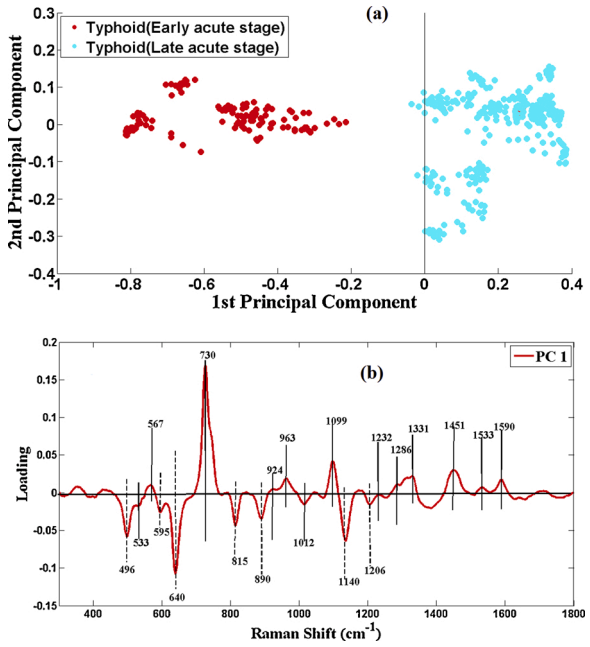


Fig. 4. (a) PCA Scatter plot of SERS spectral data of early acute stage (red) compared with the late acute stage (cyan) (b) Loadings of PCA of early acute stage compared with late acute stage of typhoid serum samples.

cm^{-1}, 595 cm^{-1}, 640 cm^{-1}, 782 cm^{-1}, 815 cm^{-1}, 890 cm^{-1}, 1144 cm^{-1}, 1285 cm^{-1}, and 1362 cm^{-1} can be linked with the Raman spectra of late acute stage typhoid samples, clustered in the negative side of the x-axis. Major variations are explained by PC-1 as 78 % and the remaining 22 % explained by PC-2. The results of the loadings confirm the findings made based on the mean spectra (Fig. 1) of the infected serum samples and healthy ones.

The loading plots for PCA of healthy and typhoid samples either early acute stage and late acute stage are very much similar because in this case, the peaks majorly contributing to differentiate samples on the positive and negative axis of PC-1 are mostly the SERS characteristic features associated with the typhoid development and those peaks have formerly been mentioned in the mean spectra. The peaks related to healthy samples are on the positive axis of PC-1 loadings and are exactly similar in both cases and the bands that are associated with typhoid development (early acute/late acute stage) are on the negative axis of PC-1 loadings and they are also quite similar but few minor changes can be seen (Figs. 2b and 3b). The peak at 1625 cm^{-1} is only present in the loading plot of healthy versus early acute stage (Fig. 2 (b)) and the intensity of peaks at 496 cm^{-1} and 630 cm^{-1} is lower as compared to Fig. 3 (b). In the loadings plot, not only the peak position on the negative or positive axis is important but also the intensity of peaks is important. The peaks associated with typhoid are the same but which peak is contributing more in the early acute stage and which one contributing more in the late acute stage is mainly associated with the intensity of positive and negative loadings. That is why, to better see which SERS features are related to the early acute stage of typhoid and which features are related to late acute stage typhoid, PCA scores plot and loading plot has been plotted between early and late acute stage as shown in Fig. 4. The SERS bands which are more intense or solely present in the early acute stage can be seen on the negative axis and the features that contribute more in the late acute stage of typhoid can be seen on the positive axis of the PC-1 loading plot in Fig. 4 (b).

In Fig. 4(a) (b), PCA scatter plot of SERS spectral data sets of two stages of typhoid including early acute stage (red dots) compared with the late acute stage of typhoid (cyan dots) and shows that both sets of SERS spectral data are clustered in the negative and positive axis of PC-1, respectively showing considerable differentiation. The reason of this differentiation is indicated in the form of positive loadings including 567 cm^{-1}, 730 cm^{-1}, 924 cm^{-1}, 963 cm^{-1}, 1099 cm^{-1}, 1232 cm^{-1}, 1286 cm^{-1}, 1331 cm^{-1}, 1451 cm^{-1}, 1533 cm^{-1} and 1590 cm^{-1} can be related with the Raman spectra features of late acute stage of typhoid serum samples grouped in the positive axis of the PC-1 and loading in negative side including 496 cm^{-1}, 533 cm^{-1}, 595 cm^{-1}, 640 cm^{-1}, 815 cm^{-1}, 890 cm^{-1}, 1012 cm^{-1} 1140 cm^{-1} and 1206 cm^{-1} which can be linked with the Raman spectral data points of early acute stage of typhoid serum samples which is clustered in the negative side of the PC-1. Major

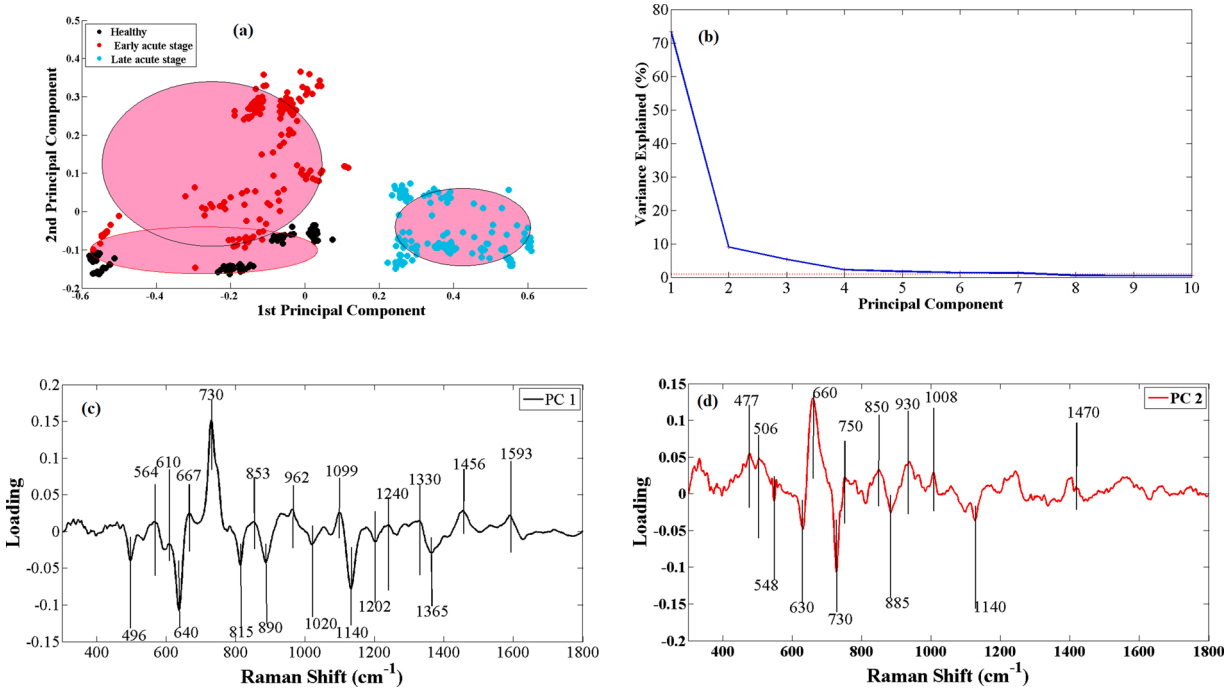


Fig. 5. (a) PCA scatter plot of SERS spectral data set healthy compared with both stages early acute stage (red) and late acute stage (cyan) typhoid. (b) Scree plot of healthy versus various stages of typhoid. (c) Loading PC-1 and (d) loading PC-2.

Table 2
Evaluation parameters of PLS-DA model for SERS spectral data sets.

SERS Spectral Datasets	Latent Variables	Sensitivity (%)	Specificity (%)	Accuracy (%)	AUROC
Healthy Vs early acute stage	18	100	100	100	0.87
Healthy Vs late acute stage	16	89	97	91	0.52

variability is explained by PC-1 as 70 % leaving behind the remaining 30 % explained by PC-2.

Fig. 5 (a) PCA scatter plot gave out clear differentiation between different stages of typhoid such as early acute stage (red dots), late acute stage (cyan dots), and healthy samples (black dots). Fig. 5 (b) shows the scree plot of healthy versus both stages of typhoid. Fig. 5 (c) the positive loadings including 564 cm^{-1}, 610 cm^{-1}, 667 cm^{-1}, 730 cm^{-1}, 853 cm^{-1}, 962 cm^{-1}, 1099 cm^{-1}, 1240 cm^{-1}, 1330 cm^{-1}, 1456 cm^{-1} and 1593 cm^{-1} can be related with the Raman spectra of healthy serum samples, grouped in the positive axis of the PC-1 and loadings in negative side including 496 cm^{-1}, 640 cm^{-1}, 815 cm^{-1}, 890 cm^{-1}, 1144 cm^{-1}, 1140 cm^{-1}, 1202 cm^{-1}, and 1365 cm^{-1} can be linked with the Raman spectra of late acute stage typhoid samples, clustered in the negative side of the x-axis. Major variations are explained by (c) PC-1 as 73 % and the remaining 9 % is explained by PC-2 (d).

3.2. Partial least square-discriminant analysis (PLS-DA)

PLS-DA model was built by using SERS spectral data and finding the optimal number of latent variables [63]. Although PCA-DA and PLS-DA both are dimensionality reduction methods, PCA-DA has the ability to reduce the dimensionality of the SERS data set in order to maintain information for small number of class. If this technique is used for large number of classes then such a setting will lose much information. In order to retain information for large number of classes, the PLS-DA classifier model has been used for reducing the dimensionality of hyperspectral datasets as well as determining the optimal subset of latent variables to produce the highest classification accuracies. In previous studies, PLS-DA has found to give good results as compared to PCA-LDA [64]. Another reason to choose the PLS-DA model for classification is that it explains variability within the group to a greater extent as compared to variability among the group. Furthermore, it is a recognition tool having the potential to explain outliers. It is the best fit model to classify given data sets when there is no knowledge about the variability range among the groups [65]. The whole was randomized first and then into the calibration dataset (60 %) and the validation dataset (40 %) to avoid any biasedness in the data. The calibration dataset was used to build the model and yes, leave one Patient out cross-validation has been performed along with it to choose the optimal number of latent variables. The built model was applied to the validation dataset to check the performance of the established model. In the current study, the PLS-DA model was applied for serum samples of healthy versus two stages of typhoid serum including early acute and late acute stages. Classification among healthy and two stages of typhoid was further explained by calculating Receiver Operating Curve (ROC) from SERS spectral data sets.

The value 1 for the area under curve of ROC is an indication of good performance of the PLS-DA model and a value equal to zero shows poor performance of this classifier model. Receiver Operating Curve is the plot of true positive rate (sensitivity) and false positive rate (1- specificity). Table 2 shows the evaluation parameters of the PLS-DA model for SERS spectral data sets of healthy versus early acute stage and healthy versus late acute stage. The value of Area under Curve for healthy versus early acute stage is found to be 0.87 and that for healthy versus late acute stage is found to be 0.52. Latent variables used for SERS spectral data sets of healthy vs. early acute stage and healthy vs. late acute stage were 18 and 16, respectively.

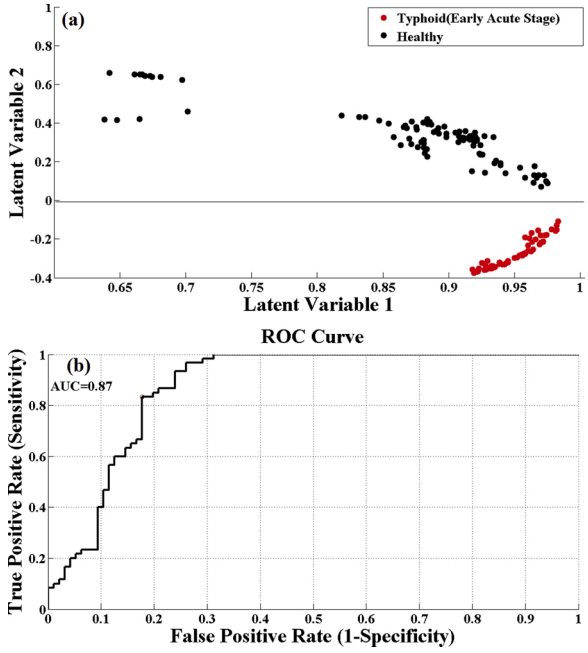


Fig. 6. (a) Scores plot of the classified model, PLS-DA, for healthy serum (healthy dots above the straight line) versus early acute stage of typhoid serum samples (red dots below the straight line). (b) Area under curve (AUC) of the healthy and early acute stage of typhoid.

4. Discussion

To investigate the capability of Surface-enhanced Raman Spectroscopy (SERS) to identify the spectral features associated with the biochemical changes taking place during the development of the severity of infectious diseases such as typhoid at an early stage and late acute stage in comparison with healthy serum, SERS has been performed. The spectral features including 496 cm^{-1} (glycogen), 533 cm^{-1} (cholesterol ester), 595 cm^{-1} (phosphatidylinositol), 730 cm^{-1} (lipids), 815 cm^{-1} (collagen assignments), 1005 cm^{-1} (phenylalanine), 1099 (palmitic acid) cm^{-1}, 1140 cm^{-1} (Alpha-amylase), 1330 cm^{-1} (associated with DNA and phospholipids collagen) and 1455 cm^{-1} (deoxyribose) are observed as striking features and used as spectral markers for the diagnosis of typhoid. Serum lipid profile studies have shown that levels of cholesterol, triacyl glycerides, and lipids in individuals diagnosed with typhoid are significantly elevated [66]. This rise of levels of cholesterol is manifested in the form of typhoid-associated cardiovascular complications [67]. SERS bands observed at 640 cm^{-1} are reported for the presence of uric acid [68]. After ingestion, *Salmonella* resides in the Peyer's patches (PP) and spread throughout the body, and colonizes in reticuloendothelial tissues leading to cytokine secretion by macrophages against bacterial by-products. This event, with many other factors, leads to release a large number of biological compounds in body fluids including the adenosine deaminase (ADA) enzyme [69]. ADA is involved in irreversible catalysis and hydrolytic deamination of adenosine to uric acid. The increased level of ADA indicates this enzyme's significance in cell proliferation, to prevent accumulation of toxic metabolite [70]. So, it is suggested that these could have originated because of higher uric acid concentration. Raman peak at 838 cm^{-1} represents optical signature of tyrosine [71]

Lipid characteristic peak at wavenumber 730 cm^{-1} is observed [57] 1099 cm^{-1} (palmitic acid) [58] 1399 cm^{-1} and 1556 cm^{-1} represents

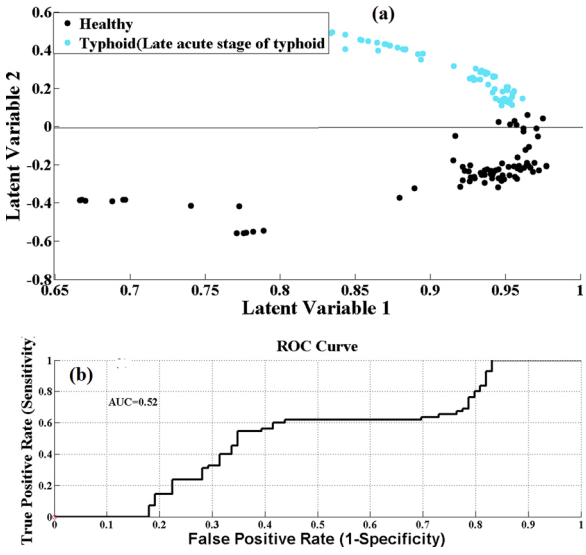


Fig. 7. (a) Scores plot of PLS-DA classified model for healthy serum (black dots below the straight line) vs. late acute stage of typhoid serum (cyan dots above the straight line). (b) Area under curve (AUC) of the healthy and late acute stage of typhoid.

high density lipoproteins (HDL) [59]. Studies have revealed that elevated levels of lipids, very low density lipoproteins (vLDL), high density lipoproteins (HDL), low density lipoproteins (LDL), and triacylglycerols are associated with the cardiovascular status of typhoid patients, as these molecules promote the development of atheroma, which leads to myocardial infarction, peripheral vascular disease and stroke [72]. Mean plasma, serum, and urine levels of amylase are reported to increase in typhoid patients as a manifestation of pancreatitis [73]. *S. typhi* is included in the list of pathogens implicating non-alcoholic pancreatitis. This band shows the greater intensity of typhoid positive serum as pancreatitis due to bacterial etiology has been documented in the literature that leads to an elevation of the mean serum and amylase levels in the urine [74]. At 1330 cm^{-1}, a band is observed in the mean SERS spectrum of typhoid serum samples and represents CH_3 and CH_2 wagging (proteins/lipids) [60]. As described earlier, lipid profiles are significantly altered in typhoid patients and are manifested as typhoid-related cardiovascular complications [66]. Defense protein levels that play a role in clearing bacteria and preventing spleen and liver infection from spreading are also known to increase in cases of typhoid infections [75]. Like many other infections, *Salmonella typhi* causes sepsis and apoptosis in many cells by activating toll receptors that are the basis of cell-free DNA in the serum. SERS signatures in case of certain diseases are known as cell-free DNA [76]. The above discussed SERS features can be associated with the development of the typhoid disease and biochemical changes as a result of this, taking place in the serum samples, which can be used to diagnose typhoid infection in human serum [41]. The scatter plot (PCA) of various samples is helpful to explain variability among different samples and among same group of samples as indicated in (Fig. 2 (a) & (b)). As found in the mean SERS spectra (Fig. 1), the bands used to distinguish biochemical changes associated with typhoid fever are also identified in the PCA loadings. Principal component 1 and principal component 2 loadings plots are generated using principal component analysis and explain the separation of disease and healthy samples based on spectral differences. Loadings, more pronounced at some variations due to spectral variation in that region. Therefore, it is concluded that principal component analysis accurately captures alterations in bimolecular distributions and successfully clusters the two kinds of datasets centered on the subtle difference in concentration of biomolecules. In Figs. 5 and 6, the PLS-DA classifier model gives accuracy, sensitivity, and specificity of 1 for healthy vs. early acute stage of typhoid SERS spectral data set. PLS-DA classifier model gives values of 0.91, 0.89, and 0.97 for accuracy, sensitivity, and specificity, respectively for SERS spectral data sets of healthy versus late acute stage. The maximum value of Area under Curve (AUC) equal or near to 1indicated that PLS-DA classifier model shows good performance of this model (Fig. 7).

5. Conclusion

Surface-Enhanced Raman spectroscopy (SERS) provides a reliable way to diagnose typhoid, an infectious disease, due to its high accuracy, sensitivity, and specificity. SERS is useful to differentiate between healthy and two different stages of typhoid including early and late acute stages. Principle component analysis (PCA) is found to be helpful in analyzing the variability among different groups of SERS spectral data sets. Furthermore, the PLS-DA classifier model was applied to check the accuracy, specificity, and sensitivity of this analytical tool for the SERS spectral dataset acquired from serum samples of healthy versus two stages of typhoid. PLS-DA classifier model gives accuracy, sensitivity, and specificity of 1 for healthy vs. early acute stage of typhoid SERS spectral data set. PLS-DA classifier model gives values of 0.91, 0.89, and 0.97 for accuracy, sensitivity, and specificity, respectively for SERS spectral data sets of healthy versus late acute stage. These results prove the potential of SERS for the characterization of biochemical changes associated with the development of typhoid and the severity of this infectious disease at an early stage.

Declaration of Competing Interest

The authors report no declarations of interest.

Acknowledgments

This work was supported by the Higher Education Commission (HEC) of Pakistan [Grants # 8494/NRPU and 6400/NRPU].

Appendix A. Supplementary data

Supplementary material related to this article can be found, in the online version, at doi:https://doi.org/10.1016/j.pdpdt.2021.102329.

References

[1] T. Pang, Genetic dynamics of Salmonella typhi—diversity in clonality, Trends Microbiol. 6 (9) (1998) 339–342.
[2] S. Hosoglu, M. Aldemir, S. Akalin, M.F. Geyik, I.H. Tacyildiz, M. Loeb, Risk factors for enteric perforation in patients with typhoid fever, Am. J. Epidemiol. 160 (1) (2004) 46–50.
[3] C. Ansong, H. Yoon, A.D. Norbeck, J.K. Gustin, J.E. McDermott, H.M. Mottaz, J. Rue, J.N. Adkins, F. Heffron, R.D. Smith, Proteomics analysis of the causative agent of typhoid fever, J. Proteome Res. 7 (2) (2008) 546–557.
[4] B. Veeraraghavan, A.K. Pragasam, Y.D. Bakthavatchalam, R. Ralph, Typhoid fever: issues in laboratory detection, treatment options & concerns in management in developing countries, Future Sci. OA 4 (6) (2018) 12.
[5] M. Ali, A. Yahaya, F. Nas, A. Anas, I. Ibrahim, Trends in treatment and vaccine development of typhoid fever: a review, Asian J. Biotechnol. Bioresour. Technol. (2017) 1–7.
[6] J.R. Andrews, K.G. Prajapati, E. Eypper, P. Shrestha, M. Shakya, K.R. Pathak, N. Joshi, P. Tiwari, M. Risal, S. Koirala, A. Karkey, S. Dongol, S. Wen, A.B. Smith, D. Maru, B. Basnyat, S. Baker, J. Farrar, E.T. Ryan, E. Hohmann, A. Arjyal, Evaluation of an electricity-free, culture-based approach for detecting typhoidal Salmonella bacteremia during enteric fever in a high burden, resource-limited setting, PLoS Negl. Trop. Dis. 7 (6) (2013) 8.
[7] Y.X. Goay, K.L. Chin, C.L.L. Tan, C.Y. Yeoh, J.N. Ja'afar, A.R. Zaidah, S.V. Chinni, K.K. Phua, Identification of five novel Salmonella Typhi-Specific genes as markers for diagnosis of typhoid fever using single-gene target PCR assays, Biomed Res. Int. (2016) 9.
[8] A.P.H. Association, Typhoid Fever and Paratyphoid Fevers, Control of Communicable Diseases Manual, 20th edition, American Public Health Association, 2015, pp. 654–660.
[9] S. Jain, S. Chattopadhyay, R. Jackeray, C.Z. Abid, G.S. Kohli, H. Singh, Highly sensitive detection of Salmonella typhi using surface aminated polycarbonate membrane enhanced-ELISA, Biosens. Bioelectron. 31 (1) (2012) 37–43.

[10] Y.W. Hartati, S. Wyantuti, M.L. Firdaus, N. Auliany, R. Surbakti, S. Gaffar, A rapid and sensitive diagnosis of typhoid fever based on nested PCR-voltammetric DNA biosensor using flagellin gene fragment, Indones. J. Chem. 16 (1) (2016) 87–91.
[11] S. Bertrand, G.D.L. de Bex, C. Wildemauwe, O. Lunguya, M.F. Phoba, B. Ley, J. Jacobs, R. Vanhoof, W. Mattheus, Multi locus variable-number tandem repeat (MLVA) typing tools improved the surveillance of Salmonella enteritidis: a 6 years retrospective study, PLoS One 10 (2) (2015) 13.
[12] J. Castonguay-Vanier, V. Davong, L. Bouthasavong, D. Sengdetka, M. Simmalavong, A. Seupsavith, D.A.B. Dance, S. Baker, L.T.P. Tu, M. Vongsouvath, P.N. Newton, Evaluation of a simple blood culture amplification and antigen detection method for diagnosis of Salmonella enterica serovar typhi bacteremia, J. Clin. Microbiol. 51 (1) (2013) 142–148.
[13] Ma. Fadeel, J.A. Crump, F.J. Mahoney, I.A. Nakhla, A.M. Mansour, B. Reyad, D. El melegi, Y. Sultan, E.D. Mintz, W.F. Bibb, Rapid diagnosis of typhoid fever by Enzyme-linked immunosorbent assay detection of salmonella serotype typhi antigens in urine, Am. J. Trop. Med. Hyg. 70 (3) (2004) 323–328.
[14] W. Chaicumpa, Y. Ruangkunaporn, D. Burr, M. Chongsa-Nguan, P. Echeverria, Diagnosis of typhoid fever by detection of Salmonella typhi antigen in urine, J. Clin. Microbiol. 30 (9) (1992) 2513.
[15] M. Xu, R. Wang, Y. Li, Rapid detection of Escherichia coli O157: H7 and Salmonella typhimurium in foods using an electrochemical immunosensor based on screen-printed interdigitated microelectrode and immunomagnetic separation, Talanta 148 (2016) 200–208.
[16] H. Frickmann, D.F. Wiemer, L. Wassill, R. Hinz, S. Rojak, A. Wille, U. Loderstadt, N. G. Schwarz, V. von Kalckreuth, J. Im, H.J. Jeon, F. Marks, E. Owusu-Dabo, N. Sarpong, J. May, D. Eibach, D. Dekker, Loop-mediated isothermal amplification-based detection of typhoid fever on an automated Genie II Mk2 system - A case-control-based approach, Acta Trop. 190 (2019) 293–295.
[17] B.H. Park, S.J. Oh, J.H. Jung, G. Choi, J.H. Seo, E.Y. Lee, T.S. Seo, An integrated rotary microfluidic system with DNA extraction, loop-mediated isothermal amplification, and lateral flow strip based detection for point-of-care pathogen diagnostics, Biosens. Bioelectron. 91 (2017) 334–340.
[18] J. Hu, Y.Z. Jiang, M. Tang, L.L. Wu, H.Y. Xie, Z.L. Zhang, D.W. Pang, Colorimetric-fluorescent-Magnetic nanosphere-based multimodal assay platform for Salmonella detection, Anal. Chem. 91 (1) (2019) 1178–1184.
[19] R. Kumar, P.K. Surendran, N. Thampuran, An eight-hour PCR-based technique for detection of Salmonella serovars in seafood, World J. Microbiol. Biotechnol. 24 (5) (2008) 627–631.
[20] I.U. Khan, S. Sajid, A. Javed, S. Sajid, S.U. Shah, Comparative diagnosis of typhoid fever by polymerase chain reaction and widal test in Southern Districts (Bannu, Lakki Marwat and DI Khan) of Khyber Pakhtunkhwa, Pakistan, Acta Sci. Malaysia 1 (2) (2017) 12–15.
[21] S.A. Schroeder, Interpretation of serologic tests for typhoid fever, JAMA 206 (4) (1968) 839–840.
[22] S.L. Hoffman, N.H. Punjabi, R.C. Rockhill, A. Sutomo, A.R. Rivai, S.P. Pulungsih, Duodenal string-capsule culture compared with bone-marrow, blood, and rectal-swab cultures for diagnosing typhoid and paratyphoid fever, J. Infect. Dis. 149 (2) (1984) 157–161.
[23] F. Schenk, P. Weber, J. Vogler, L. Hecht, A. Dietzel, G. Gauglitz, Development of a paper-based lateral flow immunoassay for simultaneous detection of lipopolysaccharides of Salmonella serovars, Anal. Bioanal. Chem. 410 (3) (2018) 863–868.
[24] N. Cheng, Y. Song, M.M. Zeinhom, Y.-C. Chang, L. Sheng, H. Li, D. Du, L. Li, M.-J. Zhu, Y. Luo, Nanozyme-mediated dual immunoassay integrated with smartphone for use in simultaneous detection of pathogens, ACS Appl. Mater. Interfaces 9 (46) (2017) 40671–40680.
[25] S. Stöckel, J. Kirchhoff, U. Neugebauer, P. Rösch, J. Popp, The application of Raman spectroscopy for the detection and identification of microorganisms, J. Raman Spectrosc. 47 (1) (2016) 89–109.
[26] H. Yao, Y. Liao, A. Lingley, A. Afanasiev, I. Lähdesmäki, B. Otis, B. Parviz, A contact lens with integrated telecommunication circuit and sensors for wireless and continuous tear glucose monitoring, J. Micromechanics Microengineering 22 (7) (2012), 075007.
[27] K. Naseer, M. Saleem, J. Qazi, Optical diagnosis of typhoid infection in human blood sera using Raman spectroscopy, Spectrosc. Lett. 53 (4) (2020) 249–255.
[28] M.K. Tuck, D.W. Chan, D. Chia, A.K. Godwin, W.E. Grizzle, K.E. Krueger, W. Rom, M. Sanda, L. Sorbara, S. Stass, W. Wang, D.E. Brenner, Standard operating procedures for serum and plasma collection: early detection research network consensus statement standard operating procedure integration working group, J. Proteome Res. 8 (1) (2009) 113–117.
[29] M. Kashif, M.I. Majeed, M.A. Hanif, Au. Rehman, Surface enhanced Raman Spectroscopy of the serum samples for the diagnosis of Hepatitis C and prediction of the viral loads, Spectrochim. Acta A. Mol. Biomol. Spectrosc. 242 (2020), 118729.
[30] H. Fang, X. Zhang, S.J. Zhang, L. Liu, Y.M. Zhao, H.J. Xu, Ultrasensitive and quantitative detection of paraquat on fruits skins via surface-enhanced Raman spectroscopy, Sens. Actuators B Chem. 213 (2015) 452–456.
[31] H. Zhou, D. Yang, N.P. Ivleva, N.E. Mircescu, Sr. Schubert, R. Niessner, A. Wieser, C. Haisch, Label-free in situ discrimination of live and dead bacteria by surface-enhanced Raman scattering, Anal. Chem. 87 (13) (2015) 6553–6561.
[32] W.W. Wilson, M.M. Wade, S.C. Holman, F.R. Champlin, Status of methods for assessing bacterial cell surface charge properties based on zeta potential measurements, J. Microbiol. Methods 43 (3) (2001) 153–164.
[33] H. Nawaz, N. Rashid, M. Saleem, M. Asif Hanif, M. Irfan Majeed, I. Amin, M. Iqbal, M. Rahman, O. Ibrahim, S. Baig, Prediction of viral loads for diagnosis of Hepatitis C infection in human plasma samples using Raman spectroscopy coupled with partial least squares regression analysis, J. Raman Spectrosc. 48 (5) (2017) 697–704.
[34] F. Westad, F. Marini, Validation of chemometric models–a tutorial, Anal. Chim. Acta 893 (2015) 14–24.
[35] T. Zelmanovitz, J.L. Gross, J.R. Oliveira, A. Paggi, M. Tatsch, M.J. Azevedo, The receiver operating characteristics curve in the evaluation of a random urine specimen as a screening test for diabetic nephropathy, Diabetes Care 20 (4) (1997) 516–519.
[36] S. Farquharson, C. Shende, F.E. Inscore, P. Maksymiuk, A. Gift, Analysis of 5-fluorouracil in saliva using surface-enhanced Raman spectroscopy, J. Raman Spectrosc. 36 (3) (2005) 208–212.
[37] H. Schulz, M. Baranska, Identification and quantification of valuable plant substances by IR and Raman spectroscopy, Vib. Spectrosc. 43 (1) (2007) 13–25.
[38] N. Stone, C. Kendall, J. Smith, P. Crow, H. Barr, Raman spectroscopy for identification of epithelial cancers, Faraday Discuss. 126 (2004) 141–157.
[39] N. Stone, C. Kendall, N. Shepherd, P. Crow, H. Barr, Near-infrared Raman spectroscopy for the classification of epithelial pre-cancers and cancers, J. Raman Spectrosc. 33 (7) (2002) 564–573.
[40] C. Krafft, L. Neudert, T. Simat, R. Salzer, Near infrared Raman spectra of human brain lipids, Spectrochim. Acta A Mol. Biomol. Spectrosc. 61 (7) (2005) 1529–1535.
[41] K.S. Myint, T.P. Endy, D. Mongkolsirichaikul, C. Manomuth, S. Kalayanarooj, D. W. Vaughn, A. Nisalak, S. Green, A.L. Rothman, F.A. Ennis, Cellular immune activation in children with acute dengue virus infections is modulated by apoptosis, J. Infect. Dis. 194 (5) (2006) 600–607.
[42] C.J. Frank, R.L. McCreery, D.C. Redd, Raman spectroscopy of normal and diseased human breast tissues, Anal. Chem. 67 (5) (1995) 777–783.
[43] W.T. Cheng, M.T. Liu, H.N. Liu, S.Y. Lin, Micro-Raman spectroscopy used to identify and grade human skin pilomatrixoma, Microsc. Res. Tech. 68 (2) (2005) 75–79.
[44] E. Hanlon, R. Manoharan, T.W. Koo, K. Shafer, J. Motz, M. Fitzmaurice, J. Kramer, I. Itzkan, R. Dasari, M. Feld, Prospects for in vivo Raman spectroscopy, Phys. Med. Biol. 45 (2) (2000) R1.
[45] H. EB, K. TW, S. KE, Prospects for in Vivo Raman Spectroscopy, 2000.
[46] L. Silveira Jr., S. Sathaiah, R.A. Zângaro, M.T. Pacheco, M.C. Chavantes, C. A. Pasqualucci, Correlation between near-infrared Raman spectroscopy and the histopathological analysis of atherosclerosis in human coronary arteries, Lasers Surg. Med. 30 (4) (2002) 290–297.
[47] I. Notingher, C. Green, C. Dyer, E. Perkins, N. Hopkins, C. Lindsay, L.L. Hench, Discrimination between ricin and sulphur mustard toxicity in vitro using Raman spectroscopy, J. R. Soc. Interface 1 (1) (2004) 79–90.
[48] J. Binoy, J.P. Abraham, I.H. Joe, V. Jayakumar, G. Pettit, O.F. Nielsen, NIR-FT Raman and FT-IR spectral studies and ab initio calculations of the anti-cancer drug combretastatin-A4, J. Raman Spectrosc. 35 (11) (2004) 939–946.
[49] I. ur Rehman, Z. Movasaghi, S. Rehman, Vibrational Spectroscopy for Tissue Analysis, CRC press, 2012.
[50] C.D. Syme, The Analysis of Raman Optical Activity Spectra of Proteins, University of Glasgow, 2002.
[51] R. Malini, K. Venkatakrishna, J. Kurien, K.M. Pai, L. Rao, V. Kartha, C.M. Krishna, Discrimination of normal, inflammatory, premalignant, and malignant oral tissue: a Raman spectroscopy study, Biopolymers: Original Res. Biomol. 81 (3) (2006) 179–193.
[52] G. Shetty, C. Kendall, N. Shepherd, N. Stone, H. Barr, Raman spectroscopy: elucidation of biochemical changes in carcinogenesis of oesophagus, Br. J. Cancer 94 (10) (2006) 1460–1464.
[53] A. Ruiz-Chica, M. Medina, F. Sanchez-Jimenez, F. Ramirez, Characterization by Raman spectroscopy of conformational changes on guanine–cytosine and adenine–thymine oligonucleotides induced by aminooxy analogues of spermidine, J. Raman Spectrosc. 35 (2) (2004) 93–100.
[54] Y.K. Min, T. Yamamoto, E. Kohda, T. Ito, H.O. Hamaguchi, 1064 nm near-infrared multichannel Raman spectroscopy of fresh human lung tissues, J. Raman Spectrosc. 36 (1) (2005) 73–76.
[55] J. Taboury, J. Liquier, E. Taillandier, Characterization of DNA structures by infrared spectroscopy: double helical forms of poly (dG-dC)• poly (dG-dC), poly (dD8G-dC)• poly (dD8G-dC), and poly (dG-dm5C)• poly (dG-dm5C), Can. J. Chem. 63 (7) (1985) 1904–1909.
[56] Z. Movasaghi, S. Rehman, I.U. Rehman, Raman spectroscopy of biological tissues, Appl. Spectrosc. Rev. 42 (5) (2007) 493–541.
[57] L. Sitole, F. Steffens, D. Meyer, Raman spectroscopy-based metabonomics of HIV-infected sera detects amino acid and glutathione changes, Curr. Metabolomics 3 (1) (2015) 65–75.
[58] J. De Gelder, K. De Gussem, P. Vandenabeele, L. Moens, Reference database of Raman spectra of biological molecules, J. Raman Spectrosc 38 (9) (2007) 1133–1147.
[59] P. Knief, C. Clarke, E. Herzog, M. Davoren, F.M. Lyng, A.D. Meade, H.J. Byrne, Raman spectroscopy–a potential platform for the rapid measurement of carbon nanotube-induced cytotoxicity, Analyst 134 (6) (2009) 1182–1191.
[60] R. Borges, I. Khan, W.E. Johnson, M.T.P. Gilbert, G. Zhang, E.D. Jarvis, S. J. O'Brien, A. Antunes, Gene loss, adaptive evolution and the co-evolution of plumage coloration genes with opsins in birds, BMC Genomics 16 (1) (2015) 1–14.
[61] K. Wojtuszewski, I. Mukerji, The HU–DNA binding interaction probed with UV resonance Raman spectroscopy: structural elements of specificity, Protein Sci. 13 (9) (2004) 2416–2428.
[62] H. Najbjerg, N.K. Afseth, J.F. Young, H.C. Bertram, M.E. Pedersen, S. Grimmer, G. Vogt, A. Kohler, Monitoring cellular responses upon fatty acid exposure by

Fourier transform infrared spectroscopy and Raman spectroscopy, Analyst 136 (8) (2011) 1649–1658.
[63] J.A. Westerhuis, H.C. Hoefsloot, S. Smit, D.J. Vis, A.K. Smilde, E.J. van Velzen, J. P. van Duijnhoven, F.A. van Dorsten, Assessment of PLSDA cross validation, Metabolomics 4 (1) (2008) 81–89.
[64] W. Liu, Z. Sun, J. Chen, C. Jing, Raman spectroscopy in colorectal cancer diagnostics: comparison of PCA-LDA and PLS-DA models, J. Spectrosc. 2016 (2016).
[65] L.C. Lee, C.-Y. Liong, A.A. Jemain, Partial least squares-discriminant analysis (PLS-DA) for classification of high-dimensional (HD) data: a review of contemporary practice strategies and knowledge gaps, Analyst 143 (15) (2018) 3526–3539.
[66] J.I. Gallin, D. Kaye, W.M. O'Leary, Serum lipids in infection, N. Engl. J. Med. 281 (20) (1969) 1081–1086.
[67] A.J. Szalai, J. VanCott, J.R. McGhee, J.E. Volanakis, W.H. Benjamin, Human C-reactive protein is protective against fatal Salmonella enterica serovar typhimurium infection in transgenic mice, Infect. Immun. 68 (10) (2000) 5652–5656.
[68] E. Brindha, R. Rajasekaran, P. Aruna, D. Koteeswaran, S. Ganesan, Raman spectroscopy of bio fluids: an exploratory study for oral cancer detection, Optical Biopsy XIV: toward Real-Time Spectroscopic Imaging and Diagnosis, Int. Soc. Opt. Photonics (2016) 97031T.
[69] K. Naseer, A. Amin, M. Saleem, J. Qazi, Raman spectroscopy based differentiation of typhoid and dengue fever in infected human sera, Spectrochim. Acta A. Mol. Biomol. Spectrosc. 206 (2019) 197–201.
[70] S. Ketavarapu, G. Uma Ramani, P. Modi, A study on the serum adenosine deaminase activity in patients with typhoid fever and other febrile illnesses, J. Clin. Diagn. Res. JCDR 7 (4) (2013) 613.
[71] M.N. Siamwiza, R.C. Lord, M.C. Chen, T. Takamatsu, I. Harada, H. Matsuura, T. Shimanouchi, Interpretation of the doublet at 850 and 830 cm-1 in the Raman spectra of tyrosyl residues in proteins and certain model compounds, Biochemistry 14 (22) (1975) 4870–4876.
[72] O.Y. Ndukaku, E.U. Emmanuel, E.A. Mercy, N.O. Caroline, Evaluation of the serum liver enzyme markers, lipid profile, and kidney function parameters in typhoid patients, Int. J. Trop. Dis. Health 8 (2) (2015) 79–89.
[73] O. Idonije, O. Festus, S. Agbebaku, A Comparative assessment of serum plasma and urine amylase levels in typhoid feverand HIV/AIDS patient, Pelagra Research library, Adv. Applied Sci. Res. 4 (3) (2013) 16–22.
[74] S.E. Hearne, T.E. Whigham, C.E. Brady III, Pancreatitis and typhoid fever, Am. J. Med. 86 (4) (1989) 471–473.
[75] G. Szalai, G. Csordás, B.M. Hantash, A.P. Thomas, G. Hajnóczky, Calcium signal transmission between ryanodine receptors and mitochondria, J. Biol. Chem. 275 (20) (2000) 15305–15313.
[76] D.R.D. Andrade, D.R.D. Andrade Júnior, Typhoid fever as cellular microbiological model, Rev. Inst. Med. Trop. Sao Paulo 45 (4) (2003) 185–191.